

## THERMOMECHANICAL STRESS ANALYSIS OF THICK-WALLED CYLINDER WITH INNER FGM LAYER

## TERMOMEHANIČKA ANALIZA NAPONA DEBELOZIDNOG CILINDRA SA UNUTRAŠNJIJIM SLOJEM OD FUNKCIONALNOG KOMPOZITA

Originalni naučni rad / Original scientific paper  
UDK /UDC: 66.018:539.3

Rad primljen / Paper received: 29.08.2019

Adresa autora / Author's address:

<sup>1)</sup> Department of Mathematics, School of Technology, Pandit Deendayal Petroleum University, Gandhinagar, Gujarat, India email: [mehtaparths@gmail.com](mailto:mehtaparths@gmail.com), [manojshahani117@gmail.com](mailto:manojshahani117@gmail.com)

<sup>2)</sup> Department of Chemical Engineering, School of Technology, Pandit Deendayal Petroleum University, Gandhinagar, Gujarat, India

### Keywords

- functionally graded material (FGM)
- thick-walled cylinder
- stress-strain
- modulus of elasticity
- thermal conductivity
- thermal expansion

### Abstract

*In this paper, we have conducted finite element analysis of thick-walled sandwich cylinder with inner layer made up of functionally graded material (FGM) and outer layer as composite. The response of sandwich cylinder subjected to internal as well as external pressure and thermal loading is analysed. Material properties of FGM are tailored from inner to outer radii in an exponential form. The modulus of elasticity is decreasing from inner to outer radii in FGM, whereas thermal conductivity and coefficient of thermal expansion are increasing from inner to outer radii. Results for radial and tangential stresses as well as displacement in the sandwich cylinder with different reinforcement of SiC<sub>p</sub> in Al matrix are plotted and discussed. The effects of mechanical and thermomechanical stresses on sandwich composition of thick-walled cylinder is analysed.*

### INTRODUCTION

Functionally Graded Materials (FGMs), are an advanced class of inhomogeneous materials made with combination of metal and ceramic which provides high resistance to thermal and mechanical stresses as compared to composite materials. The advantage of functionally graded materials over traditional composites is that one can continuously vary material properties, or material volume over the dimension of the body. Such an advantage of FGMs is utilized to develop structures which can operate under high thermal and mechanical loading. By varying material properties or material volume or both, overall material strength can be improved. This innovative idea in form of FGMs started to develop in Japan (1984), by a group of scientists, who were looking for a new material which can provide high thermal resistance at temperatures as high as 2000 K across 10 mm body section with thermal gradient of 1000 K.

### Ključne reči

- functionally kompozitni materijal (FGM)
- debelozidni cilindar
- napon-deformacija
- modul elastičnosti
- provođenje toplote
- toplotno širenje

### Izvod

*U radu smo izveli analizu konačnim elementima debelozidnog cilindra sa sendvič strukturom, gde je unutrašnji sloj od funkcionalnog kompozita (FGM), a spoljni sloj je od kompozitnog materijala. Razmatran je uticaj unutrašnjeg i spoljašnjeg pritiska, kao i uticaj toplote na ponašanje sendvič cilindra. Pretpostavljene su eksponencijalne osobine FGM materijala od unutrašnjeg ka spoljnom poluprečniku. Modul elastičnosti opada od unutrašnjeg ka spoljnom poluprečniku u FGM, a toplotna provodnost i koeficijent termičkog širenja rastu od unutrašnjeg ka spoljnom poluprečniku. Predstavljani su i diskutovani rezultati radialnih i tangencijalnih napona, kao i pomeranja u sendvič cilindru, sa različitim ojačanjem tipa SiC<sub>p</sub> u Al matrici. Analizirani su uticaji mehaničkih i termomehaničkih napona na sendvič strukturu debelozidnog cilindra.*

Since then, lot of researchers conducted analysis of FGMs in order to understand its behaviour under the effect of thermal loading, mechanical loading, body loads such as centrifugal, magnetic, etc. Seifi /1/ obtained displacement and thermomechanical stress distributions in FG hollow cylinder assumed to be under high temperature and internal pressure, with power-law and exponentially varying material properties by using approximate homogeneous multilayer semi-analytical method. Malekzadeh et al. /2/ presented transient heat transfer analysis of functionally graded hollow cylinder subjected to a distributed heat flux with a moving front boundary on its inner surface using finite element and differential quadrature method for discretizing the governing equations in the spatial domain. Hajisadeghian et al. /3/ presented analytical solution for thick-walled cylinder with inner layer made up of FGM under the effect of mechanical, thermal and magnetic loading. Thawait et al. /4/ conducted finite element analyses and studied displace-

ment as well as stress in variable thickness disk made up of FGM using 4-noded quadrilateral finite element. Nie and Batra /5/ employed the Airy stress function method and derived analytical solution for plain strain static deformation of FG hollow circular cylinder with Young's modulus and Poisson's ratio varying in radial direction. Bayat et al. /6/ investigated magneto-thermo-mechanical response of functionally graded rotating disk with varying thickness along the radial direction. Mehta et al. /7/ studied the effect of varying material properties, namely elasticity modulus, density and thermal expansion in a functionally graded disc under the effect of thermal loading. Dini et al. /8/ studied magneto-thermo-elastic behaviour in functionally graded sandwich disk and presented an exact solution for stresses under the effect of internal heat generation and convective boundary condition. Yildirim et al. /9/ analysed rotating variable thickness disk under the magnetic field, centrifugal force, thermal loading and presented the distribution of stresses in radial as well as in tangential direction. Sadrabadi et al. /10/ investigated thick-walled FG cylindrical tube under thermomechanical loading and presented stress distribution to understand the effect on performance of FG cylinder by varying material properties of cylinder in power law form along the radius of cylinder. Some researchers /11-12/ also studied creep behaviour and provided analytical solution for FG cylinder under the effect of internal and external pressure. Loghman and Parsa /13/ conducted thermomechanical analysis of double walled cylinder made up of inner FGM and outer homogeneous layers, under effect of magnetic field. Researchers /14/, studied the effect of magnetic field on creep deformation in functionally graded (FG) cylinder. Celebi et al. /15/ provided a novel approach for analysis of functionally graded cylinder with exponential variation of material properties and under thermal as well as mechanical loading by employing complementary function method. Literature also provides analysis of thermomechanical behaviour of FG pressurised cylinder extended to two dimensions i.e. radial and tangential direction /16/. Taking note of above literature review, the present study deals with analysis of thick-walled cylinder which is tailored using functionally graded material with different volume content of SiC<sub>p</sub> in Al metal matrix as well as varying material properties such as elasticity modulus, thermal conductivity and thermal expansion at inner layer and homogeneous composite material at outer layer.

MATHEMATICAL FORMULATION FOR STRESS ANALYSIS OF THICK-WALLED CYLINDER

Consider a thick-walled axisymmetric cylinder with inner layer made up of FGM and outer layer from homogeneous material. The inner FG layer is made up of Al with 30, 35 and 40 % reinforcement of SiC<sub>p</sub> in radial direction, whereas outer layer is made up of Al metal matrix with 10 % reinforcement of SiC<sub>p</sub>, /3/, Fig. 1.

Material properties varying in radial direction are defined in exponential form as,

$$Y(r) = Y_F \exp \left( p_1 \left( \frac{r}{b} \right)^{m_1} \right), \tag{1}$$

$$\lambda(r) = \lambda_F \exp \left( p_2 \left( \frac{r}{b} \right)^{-m_2} \right), \tag{2}$$

$$\alpha(r) = \alpha_F \exp \left( p_3 \left( \frac{r}{b} \right)^{-m_3} \right), \tag{3}$$

where,  $Y(r)$  is Young's modulus;  $\lambda(r)$  is thermal conductivity; and  $\alpha(r)$  is thermal expansion coefficient. Also,  $m_1$ ,  $m_2$  and  $m_3$  are material property parameters, whereas  $p_1$ ,  $p_2$  and  $p_3$  are control parameters.

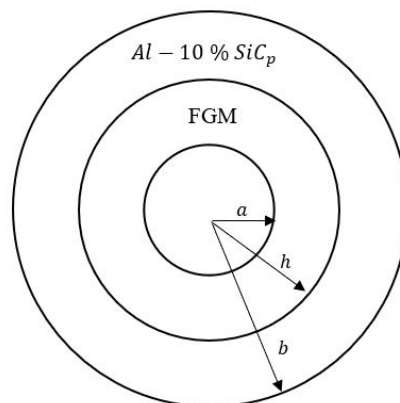


Figure 1. Thick-walled cylinder with inner FGM, and outer Al-SiC<sub>p</sub> 10 %.

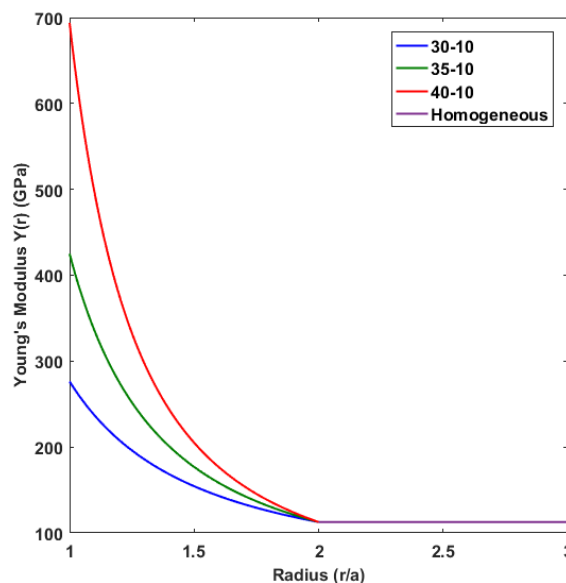


Figure 2. Young's modulus vs. radial variation.

Here in Fig. 2,  $Y(r)$  is decreasing from inner to interface radius, whereas  $\lambda(r)$  and  $\alpha(r)$  (Figs. 3 and 4) are increasing from inner to interface radius, so, Eqs.(1)-(3) hold true only by restricting radial point  $b = h$ , i.e. the interface radial point and not over the entire radius of cylinder. The FGM part of cylinder has radius from  $a = 0.1$  m to  $h = 0.2$  m, and the homogeneous part of the cylinder has radius from  $h = 0.2$  m to  $b = 0.3$  m. Material properties remain homogeneous in the outer layer of the cylinder. Here, material grading indices have different values corresponding to the type of gradation of SiC<sub>p</sub> in Al matrix. Values of all parameters and material constants are given in the results section.

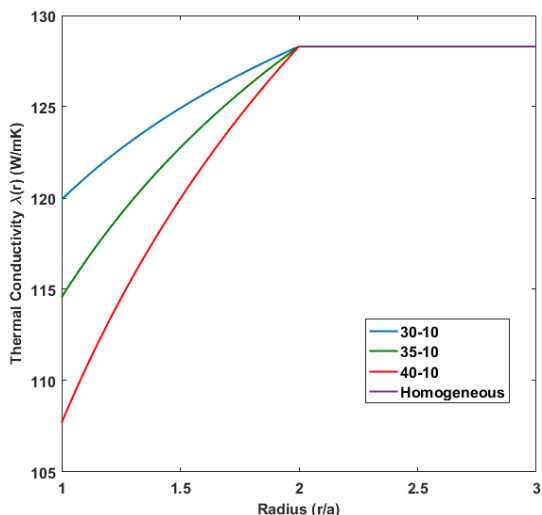


Figure 3. Thermal conductivity vs. radial variation.

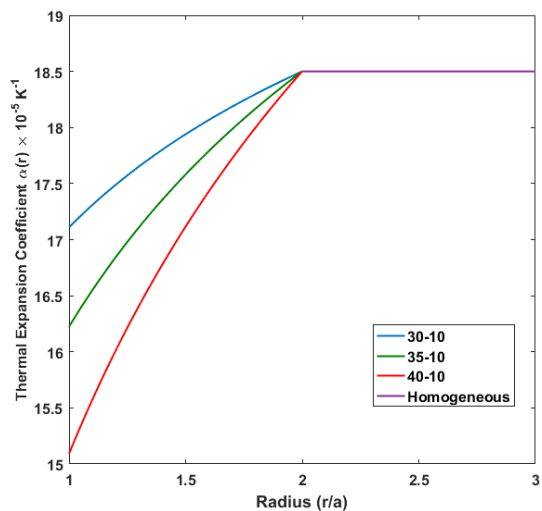


Figure 4. Thermal expansion coefficient vs. radial variation.

Governing differential equation for FG and homogeneous part of the cylinder is given by /3/,

$$\frac{d\sigma_r}{dr} + \frac{\sigma_r - \sigma_\theta}{r} = 0, \tag{4}$$

where:  $\sigma_r, \sigma_\theta$  are radial and tangential stresses, respectively, varying with radial coordinate  $r$ . The compatibility equation /2/ is given as,

$$\varepsilon_r = \frac{du}{dr} \quad \text{and} \quad \varepsilon_\theta = \frac{u}{r}, \tag{5}$$

where:  $\varepsilon_r, \varepsilon_\theta$  and  $u$  are radial strain, tangential strain, and displacement, respectively.

The compatibility condition obtained by eliminating  $u$  from the above equation is

$$\varepsilon_r = \varepsilon_\theta + r \frac{d\varepsilon_\theta}{dr}. \tag{6}$$

The constitutive relation for thermoelastic behaviour of cylinder under plane stress condition /4/ can be given as,

$$\begin{aligned} \varepsilon_r &= \frac{1}{Y_k(r)} \left[ (1-\nu_k^2)\sigma_r - \nu_k(1+\nu_k)\sigma_\theta \right] + (1+\nu_k)\alpha(r)T(r), \\ \varepsilon_\theta &= \frac{1}{Y_k(r)} \left[ (1-\nu_k^2)\sigma_\theta - \nu_k(1+\nu_k)\sigma_r \right] + (1+\nu_k)\alpha(r)T(r). \end{aligned} \tag{7}$$

On simplification, the thermoelastic relations for FG and homogeneous part of cylinder are given as,

$$\begin{aligned} \varepsilon_r &= \frac{(1-\nu_k^2)}{Y_k(r)} \left[ \sigma_r - \frac{\nu_k}{(1-\nu_k)}\sigma_\theta \right] + (1+\nu_k)\alpha(r)T(r), \\ \varepsilon_\theta &= \frac{(1-\nu_k^2)}{Y_k(r)} \left[ \sigma_\theta - \frac{\nu_k}{(1-\nu_k)}\sigma_r \right] + (1+\nu_k)\alpha(r)T(r), \end{aligned} \tag{8}$$

where:  $T(r)$  and  $\nu$  are the temperature and Poisson's ratio. Also, Poisson's ratio  $\nu = \nu_F = \nu_C = 0.3$ , where  $k = F$  or  $k = C$  represents the relation for FG and homogeneous parts of the cylinder, respectively.

From Eqs.(5) and (8) we can obtain stress components in radial and tangential direction in functionally graded and homogeneous part of cylinder /3/ given as,

$$\begin{aligned} \sigma_{r_k} &= Y_k(r)C_1\varepsilon_r + Y_k(r)C_2\varepsilon_\theta - Y_k(r)\alpha(r)T(r)C_3, \\ \sigma_{\theta_k} &= Y_k(r)C_2\varepsilon_r + Y_k(r)C_1\varepsilon_\theta - Y_k(r)\alpha(r)T(r)C_3, \end{aligned} \tag{9}$$

where:

$$C_1 = \frac{(1-\nu_k)}{(1+\nu_k)(1-2\nu_k)}, \quad C_2 = \frac{\nu_k}{(1+\nu_k)(1-2\nu_k)} \quad \text{and} \quad C_3 = \frac{1}{(1-2\nu_k)}.$$

Thermal loading in radial direction in cylinder induced by temperature difference and heat conduction, can be modelled using the heat conduction equation /3/ given as,

$$\frac{1}{r} \frac{d}{dr} \left[ r\lambda(r) \frac{dT(r)}{dr} \right] = 0, \tag{10}$$

where:  $\lambda(r)$  is the thermal conductivity variable in radial direction of FG cylinder. The temperature field  $T(r)$  can be obtained with the help of thermal conductivity given by Eq.(2) as well as the temperature difference at inner ( $a$ ) and outer ( $b$ ) radii given as,  $T(r) = T_a$  at  $r = a$  and  $T(r) = T_b$  at  $r = b$ , respectively. The temperature  $T_h$  at interface radii  $h$  can be known from heat conduction across the FG and homogeneous part of cylinder. Using Eqs.(4), (5) and (9), we obtain

$$\begin{aligned} C_1 \left[ \frac{dY}{dr} \frac{du}{dr} + Y(r) \frac{d^2u}{dr^2} \right] + C_2 \left[ \frac{dY}{dr} \frac{u}{r} + Y(r) \left( \frac{ru'(r) - u(r)}{r^2} \right) \right] - \\ - C_3 \left[ \frac{dY}{dr} \alpha(r)T(r) + \frac{d\alpha}{dr} Y(r)T(r) + \frac{dT}{dr} Y(r)\alpha(r) \right] + \\ + \left[ \frac{1}{r} \frac{du}{dr} (C_1 - C_2)Y(r) - \frac{u}{r^2} Y(r)(C_1 - C_2) \right] = 0. \end{aligned} \tag{11}$$

Due to different compositions of material at interface layer, continuity conditions in terms of radial stress and displacement in FG and homogeneous part, at boundary points  $a, b$  and at interface point  $h$  are defined as,  $\sigma_{rF}(r) = \sigma_{rC}(r) = -P_a$  at  $r = a$ ,  $\sigma_{rF}(r) = \sigma_{rC}(r)$  at  $r = h$ ,  $u_{rF}(r) = u_{rC}(r)$  at  $r = h$ ,  $\sigma_{rF}(r) = \sigma_{rC}(r) = -P_b$  at  $r = b$ .

These continuity conditions are applied as the cylinder under mechanical, as well as thermomechanical loading has different material properties varying from  $a$  to  $h$  and from  $h$  to  $b$ , and hence at interface point  $h$ , there is mismatch of stresses and displacement.

Simplifying Eq.(11) by substituting Eqs.(1) and (3) in Eq.(11) we get

$$\begin{aligned}
 & C_1 \left( \frac{Y_F e^{p_1 \left(\frac{r}{b}\right)^{m_1}} p_1 m_1 \left(\frac{r}{b}\right)^{m_1-1}}{b} \frac{du}{dr} + Y_F e^{p_1 \left(\frac{r}{b}\right)^{m_1}} \frac{d^2 u}{dr^2} \right) + C_2 \left( \frac{Y_F e^{p_1 \left(\frac{r}{b}\right)^{m_1}} p_1 m_1 \left(\frac{r}{b}\right)^{m_1-1}}{b} \frac{u}{r} + Y_F e^{p_1 \left(\frac{r}{b}\right)^{m_1}} \left( \frac{ru'(r) - u(r)}{r^2} \right) \right) - \\
 & -C_3 \left( \frac{Y_F e^{p_1 \left(\frac{r}{b}\right)^{m_1}} p_1 m_1 \left(\frac{r}{b}\right)^{m_1-1}}{b} \alpha_F e^{p_3 \left(\frac{r}{b}\right)^{-m_3}} T(r) - \frac{\alpha_F e^{p_3 \left(\frac{r}{b}\right)^{-m_3}} p_3 m_3 \left(\frac{r}{b}\right)^{-m_3-1}}{b} Y_F e^{p_1 \left(\frac{r}{b}\right)^{m_1}} T(r) + \frac{dT}{dr} Y_F e^{p_1 \left(\frac{r}{b}\right)^{m_1}} \alpha_F e^{p_3 \left(\frac{r}{b}\right)^{-m_3}} \right) + \\
 & + (C_1 - C_2) \left( \frac{1}{r} \frac{du}{dr} Y_F e^{p_1 \left(\frac{r}{b}\right)^{m_1}} - \frac{u(r)}{r^2} Y_F e^{p_1 \left(\frac{r}{b}\right)^{m_1}} \right) = 0 \tag{12}
 \end{aligned}$$

NUMERICAL SOLUTION

The above governing differential Eq.(12) is for the functionally graded part of cylinder. Considering homogeneous material properties, one can obtain a similar equation for the composite part of cylinder. Thus, equations for FG and composite part, under the prescribed continuity conditions are solved using finite element-based solver Comsol Multiphysics® (5.4). The axisymmetric geometry condition in the present geometry has been exploited for computations. The domain is discretized using triangular elements with extremely fine element size in order to capture the response of material at different radial points. For analysing thermal stresses, heat transfer module together with the solid mechanics module is used with appropriately defined pressure and temperature boundary conditions at the inner and outer radii of the cylinder geometry.

The model is solved using linear direct PARDISO® solver, capable of handling sparse matrices (real, complex, symmetric, as well as asymmetric) and provides solutions of such sparse liner system of matrices of the form AX = B. The results are computed for the cylinder with different composition of material at inner and outer layer by applying parametric sweep over material properties of the cylinder. The results for radial stress, tangential stress, displacement under different pressure and temperature cases for different compositions of cylinder with relative convergence criterion of 10<sup>-5</sup> are obtained. The accuracy of the obtained results is ensured by grid independence test. The grid test is conducted for three different grids G<sub>1</sub>, G<sub>2</sub> and G<sub>3</sub> in which the number of elements varies as 12956, 22764 and 49948, respectively. It can be seen from Figs. (5) and (6), the radial and tangential stresses under internal pressure, as well as external pressure, with thermal loading vary only with a difference in values at the sixth decimal. Thus, for the given geometry and physics involved in the present problem, G<sub>2</sub> is chosen as appropriate grid to obtain the present numerical results.

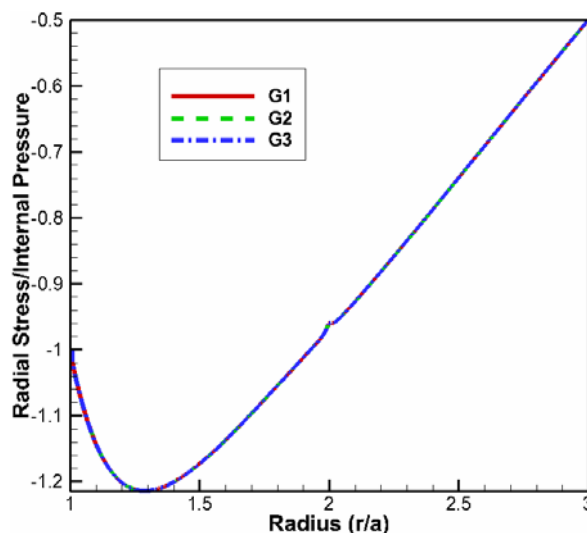


Figure 5. Radial stress for 30-10 % with  $P_a = 50$  MPa,  $P_b = 25$  MPa,  $T_a = 398$  K and  $T_b = 298$  K.

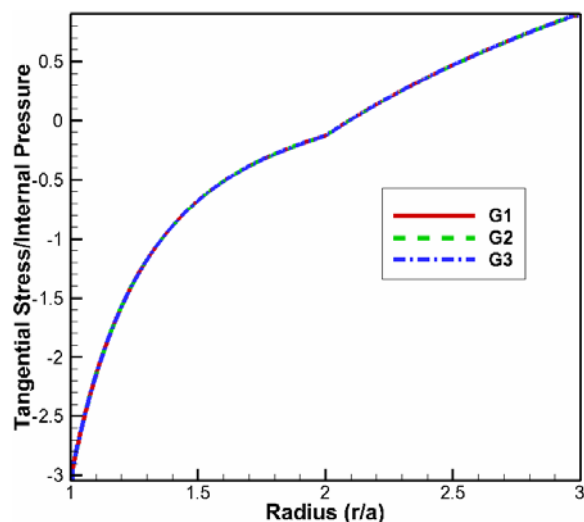


Figure 6. Tangential stress for 30-10 % with  $P_a = 50$  MPa,  $P_b = 25$  MPa,  $T_a = 398$  K and  $T_b = 298$  K.

## RESULTS AND DISCUSSION

In this section, graphs for stresses and displacement are plotted against dimensionless radius  $r/a$ . The validation of radial and tangential stresses for the case where both domains of the cylinder are homogeneous in nature is carried out as shown in Figs. (7)-(8). Stresses and displacement under the effect of mechanical and thermomechanical loading of the sandwich cylinder and their analysis are also reported. Stresses and displacement under various pressure and temperature cases are analysed thoroughly.

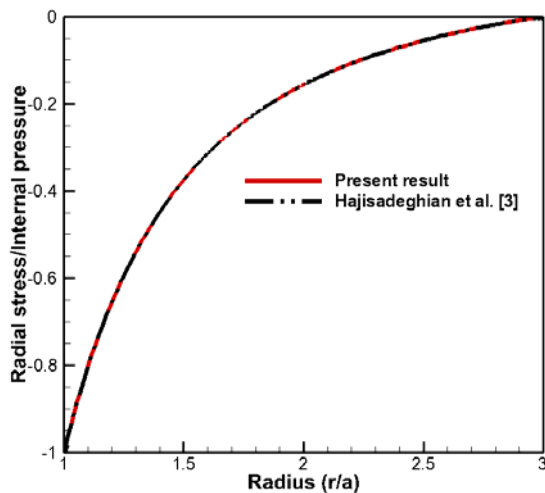


Figure 7. Radial stress for homogeneous case with  $P_a = 25$  MPa and  $T_a = T_b = 298$  K.

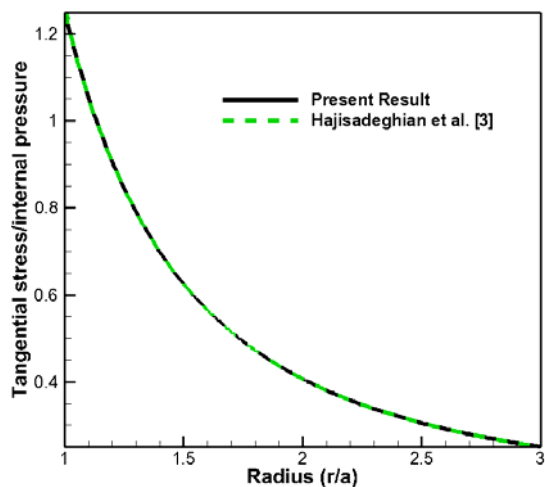


Figure 8. Tangential stress for homogeneous case with  $P_a = 25$  MPa and  $T_a = T_b = 298$  K.

The values for various profile parameters of the FG layer made up of Al metal matrix with reinforcement of  $\text{SiC}_p$  in different proportions at inner radius and 10 %  $\text{SiC}_p$  at outer radius are considered as: for 30-10 %:  $m_1 = -0.779$ ,  $m_2 = 0.236$ ,  $m_3 = 0.253$ ,  $p_1 = 1.2528$ ,  $p_2 = -0.3806$ ,  $p_3 = -0.4076$ ,  $Y_F = 32.2$  MPa,  $\lambda_F = 187.735$  W/mK and  $\alpha_F = 27.81 \cdot 10^{-6} \text{ K}^{-1}$ ; whereas for 35-10 %:  $m_1 = -0.922$ ,  $m_2 = 0.302$ ,  $m_3 = 0.324$ ,  $p_1 = 1.4834$ ,  $p_2 = -0.4864$ ,  $p_3 = -0.5215$ ,  $Y_F = 25.57$  MPa,  $\lambda_F = 208.68$  W/mK and  $\alpha_F = 31.165 \cdot 10^{-6} \text{ K}^{-1}$ ; and for 40-10 %:  $m_1 = -1.052$ ,  $m_2 = 0.371$ ,  $m_3 = 0.398$ ,  $p_1 = 1.6938$ ,  $p_2 = -0.5972$ ,  $p_3 = -0.6413$ ,  $Y_F = 20.73$  MPa,  $\lambda_F =$

233.14 W/mK and  $\alpha_F = 35.133 \cdot 10^{-6} \text{ K}^{-1}$ . Also, parameters for homogeneous material properties for the second domain made up of composite material, i.e. Al matrix reinforced with 10 %  $\text{SiC}_p$  are considered as  $Y_c = 112.7$  MPa,  $\lambda_c = 128.3$  W/mK and  $\alpha_c = 18.5 \cdot 10^{-6} \text{ K}^{-1}$ .

Figures (7) and (8) indicate that the results for radial as well as tangential stresses for the case in which both layers of the cylinder are homogeneous and the temperature conditions are  $T_a = T_b = 298$  K under the effect of internal pressure  $P_a = 25$  MPa are validated with the available result in literature, [3]. It is clear that both stresses – radial and tangential, are in close agreement as reported. These results for the homogeneous case also allow us to understand the significant contribution of FGM in terms of handling stresses. A detailed analysis of the mechanical loading and thermomechanical loading effects in the sandwich cylinder is discussed in the following sections.

## EFFECT OF MECHANICAL LOADING

Figures (9)-(20) represent the effect of mechanical loading (i.e.  $T_a = T_b = 0$ ) on sandwich cylinder with different compositions of material. It can be seen from Fig. (9) that radial stress under internal pressure  $P_a = 25$  MPa for different compositions of material is compressive at inner radial points and becomes tensile towards the interface and outer radial points. Radial stress in cylinder with 40-10 % reinforcement of  $\text{SiC}_p$  at the inner and outer radii respectively, increases in concave downward form. This effect is due to the tailoring of material properties in which the modulus of elasticity decreases from inner to interfacial radii, whereas heat conductivity and the linear coefficient of thermal expansion are increasing from inner to interfacial radii. The cylinder material with high modulus of elasticity tends to have less magnitude of stress as compared to the one with low modulus of elasticity, as it is able to withstand the mechanical loading by being more capable to resist internal forces in the cylinder.

As observed in Fig. (10), when cylinder is under external pressure  $P_b = 25$  MPa, the radial stress is highly compressive in nature from inner to outer radii. Moreover, the radial stress with 40-10 % reinforcement of  $\text{SiC}_p$  at inner and outer radii is highly compressive as compared to 30-10 %  $\text{SiC}_p$  reinforcement at inner and outer radii, in respect. As observed from Figs. (11) and (12), the radial stress under high internal  $P_a = 50$  MPa and low external pressure  $P_b = 25$  MPa in the sandwich cylinder is less compressive in nature with almost identical all composition types of cylinder, whereas in the case when the internal pressure is  $P_a = 25$  MPa and external is  $P_b = 50$  MPa, the radial stress becomes highly compressive from inner to interfacial radii, while its compressiveness decreases towards the outer radius.

Figure (13) shows tangential stress in sandwich cylinder under internal pressure  $P_a = 25$  MPa. The tangential stress with different compositions of material is tensile in nature with a decrease from inner to outer radii. It is observed that tangential stresses converge at near about  $r/a = 1.3$  to 1.4 as it tends towards the interfacial radii  $r/a = 2$ . This effect can be considered due to the variation in magnitude of tangential stresses that converge at a radial point and then spread

out towards the outer radius due to variation in modulus of elasticity. The flatter curve of tangential stress in the cylinder with 40-10 % reinforcement of  $\text{SiC}_p$  at inner and outer radii, compliments that the modulus of elasticity is higher as compared to other compositions, as it has high capacity to resist internal forces. Moreover, it can also be noted that tangential stress in cylinder with 30-10 % and 35-10 % reinforcement of  $\text{SiC}_p$  at inner and outer radii, have high tensile magnitude for tangential stress near interfacial radii towards outer radii, as the capacity to resist internal forces i.e. the modulus of elasticity is low. Also, due to material mismatching at interfacial radii, discontinuity at interfacial radii is observed. From Fig. (14), tangential stresses under external pressure  $P_b = 25$  MPa with negative values, decrease from inner to outer radii. It is also observed that tangential stress is more elastic in nature towards the outer radius. The higher magnitude of tangential stress at inner radial points is due to imposed boundary condition on radial stress which in turn contributes to tangential stress. Due to this, the tangential stress at inner radial points is higher, but towards outer radius it starts to decrease considerably, as evident from Fig. (14). Also, the effect of material mismatching is visible at interfacial radii, as there is presence of discontinuity.

Interestingly, as observed from Figs. (15)-(16), under combined effect of high internal  $P_a = 50$  MPa and low external pressure  $P_b = 25$  MPa, the tangential stresses decrease over the radius of cylinder. Also, tangential stresses with 30-10 % and 35-10 % reinforcements of  $\text{SiC}_p$  at inner and outer radii become concave at inner radius with considerable decrease, although along the outer radius its magnitude increases, resulting in further decrease in its tensile nature due to external pressure condition at outer radii. In the case when the cylinder is under effect of low internal pressure  $P_a = 25$  MPa and high external pressure  $P_b = 50$  MPa, there is an increase of tangential stresses along the radius.

Figures (17)-(20) represent the displacement in the sandwich cylinder with different material compositions. As seen in Fig. (17), displacements under the effect of internal pressure  $P_a = 25$  MPa are concave up and decrease along the cylinder radius. Displacements in cylinder with 30-10 % and 35-10 % reinforcement of  $\text{SiC}_p$  at inner and outer radii, are higher than 40-10 % reinforcement, which is attributed to the fact that radial stress is lower with 40-10 % reinforcement. Displacement under external pressure  $P_b = 25$  MPa, compresses the cylinder towards internal radii due to compressive nature of pressure at external boundary, as seen in Fig. (18). From Fig. (19) it can be noted that under combined effects of high internal  $P_a = 50$  MPa and low external pressure  $P_b = 25$  MPa, the displacements from inner to outer radius turn to compressive from tensile, confirming resisting effects due to external pressure. When external pressure increases to  $P_b = 50$  MPa, and keeping internal pressure at  $P_a = 25$  MPa, as in Fig. (20), the displacement increases from inner to outer radius of cylinder. The smoothness of displacement in the sandwich cylinder is due to continuity conditions applied at interfacial radial point for FG and the homogeneous part. Thus, from our analysis, it can be clear that displacement in sandwich cylinder with low magnitude of stress also has a low magnitude.

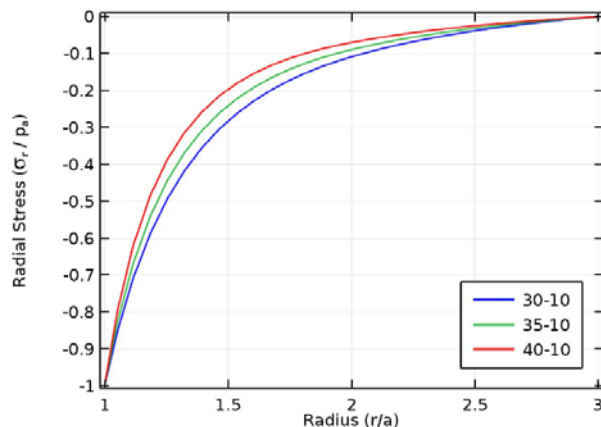


Figure 9. Radial stress under internal pressure  $P_a = 25$  MPa.

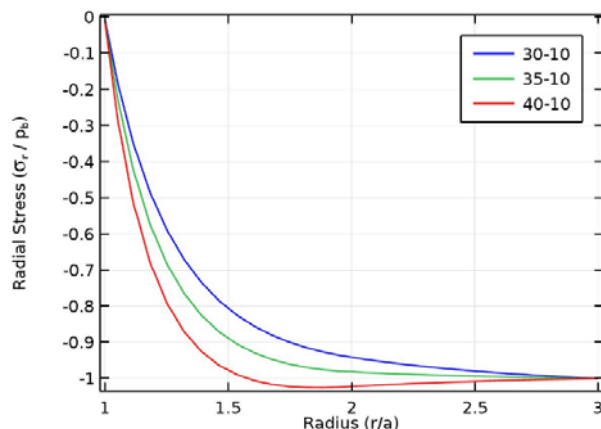


Figure 10. Radial stress under external pressure  $P_b = 25$  MPa.

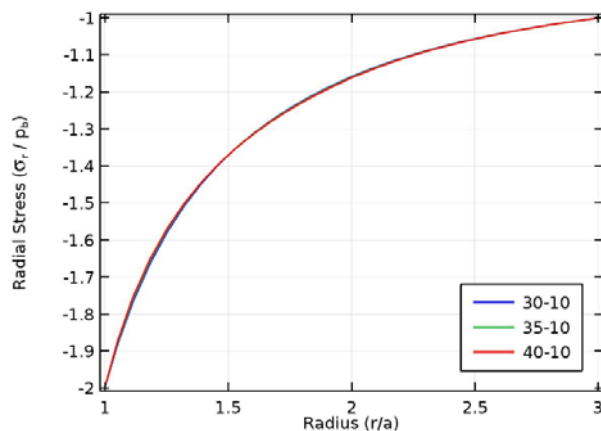


Figure 11. Radial stress with  $P_a = 50$  MPa and  $P_b = 25$  MPa.

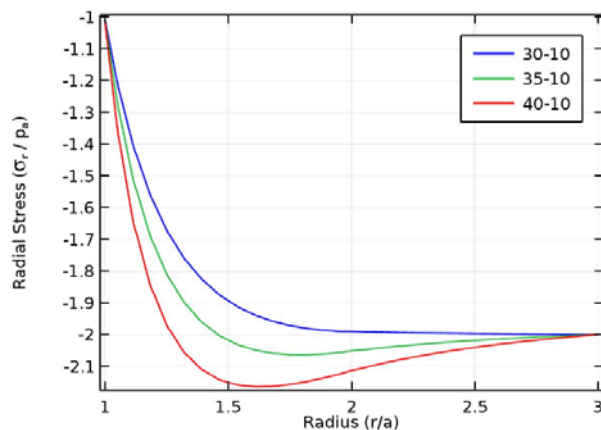


Figure 12. Radial stress with  $P_a = 25$  MPa and  $P_b = 50$  MPa.

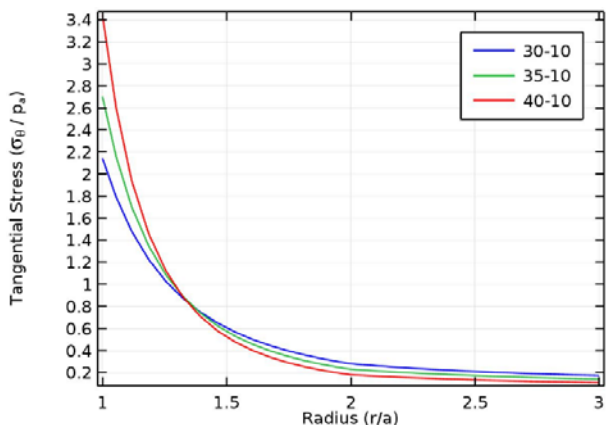


Figure 13. Tangential stress under internal pressure  $P_a = 25$  MPa.

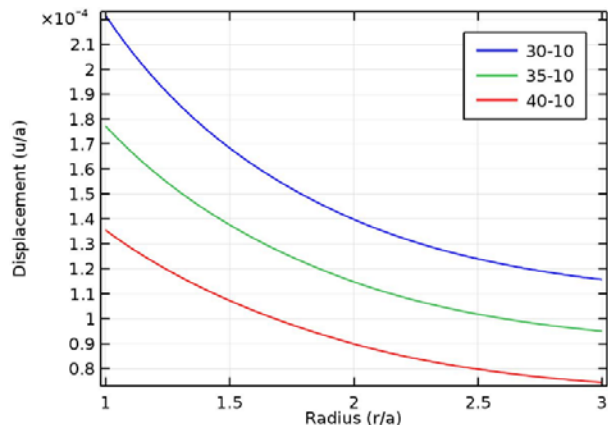


Figure 17. Displacement under internal pressure  $P_a = 25$  MPa.

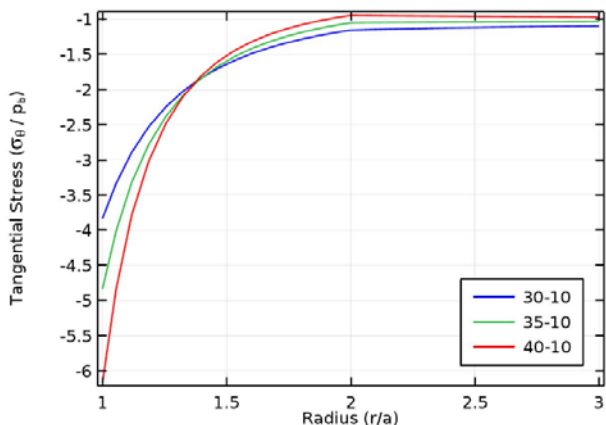


Figure 14. Tangential stress under external pressure  $P_b = 25$  MPa.

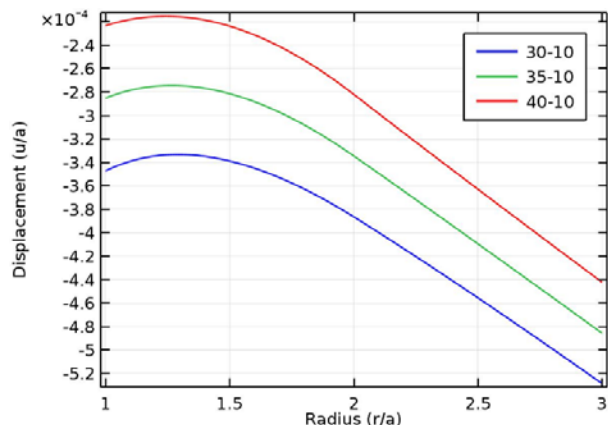


Figure 18. Displacement under external pressure  $P_b = 25$  MPa.

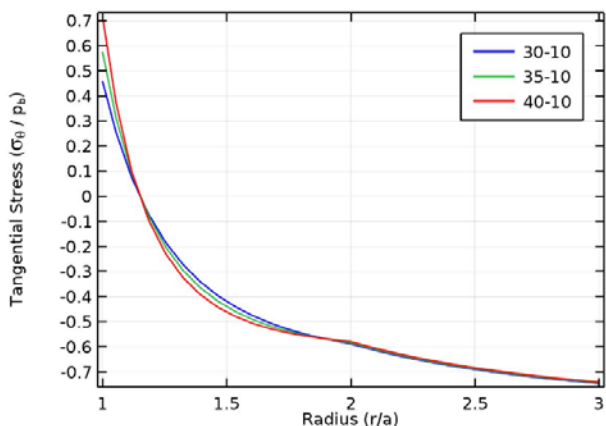


Figure 15. Tangential stress with  $P_a = 50$  MPa and  $P_b = 25$  MPa.

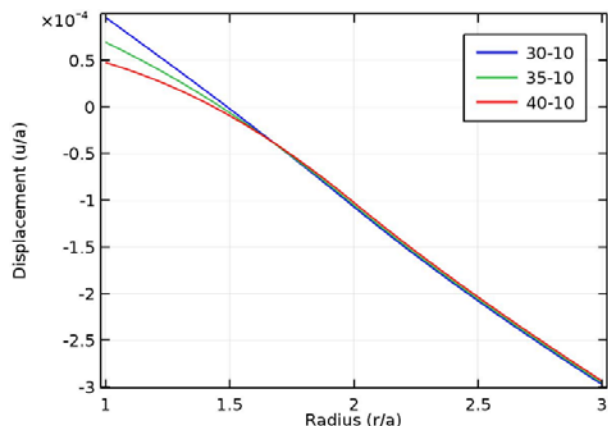


Figure 19. Displacement with  $P_a = 50$  MPa and  $P_b = 25$  MPa.

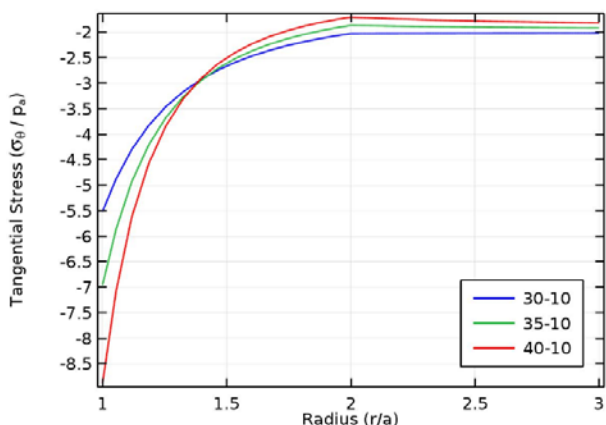


Figure 16. Tangential stress with  $P_a = 25$  MPa and  $P_b = 50$  MPa.

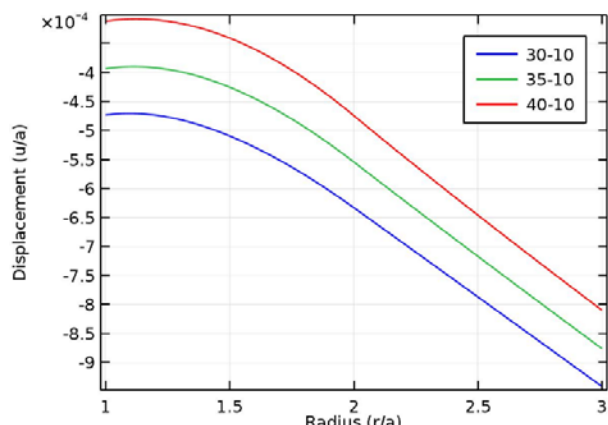


Figure 20. Displacement with  $P_a = 25$  MPa and  $P_b = 50$  MPa.

EFFECT OF THERMOMECHANICAL LOADING

The effect of thermomechanical loading on sandwich cylinder in terms of stresses and displacement is depicted in Figs. (21)-(46). Analysis is conducted under increasing and decreasing temperature profile from inner to outer radius of sandwich cylinder as shown in Figs. (21) and (34), in respect. Radial stress under increasing temperature profile from inner to outer radius with  $T_a = 298$  K,  $T_b = 398$  K, and internal pressure  $P_a = 25$  MPa for different material composition is depicted in Fig. (22). It can be observed that radial stress is compressive at inner radii and becomes tensile along the radius of the cylinder. Clearly, this change in behaviour of radial stress from compressive to tensile is due to presence of thermal loading. Also, the presence of discontinuity is clearly visible due to material mismatch at radii  $r/a = 2$ . From Fig. (23), the radial stress with thermal difference  $T_a = 298$  K,  $T_b = 398$  K and under effect of external pressure  $P_b = 25$  MPa is tensile at inner radius and becomes compressive in nature towards outer radius. When pressure is applied at both inner and outer radii, i.e.  $P_a = 50$  MPa and  $P_b = 25$  MPa, as shown in Fig. (24), there is a decrease in radial stress with tensile nature at inner, and a compressiveness at outer radius. As seen in Fig. (25), radial stress under low internal pressure  $P_a = 25$  MPa and high external pressure  $P_b = 50$  MPa, decreases from inner to outer radii. It is evident from Fig. (25), that radial stress is shifted to inner radial points due to compressive nature of pressure at external radii. Also, it has decreased as compared to the case when only external pressure is applied to sandwich cylinder.

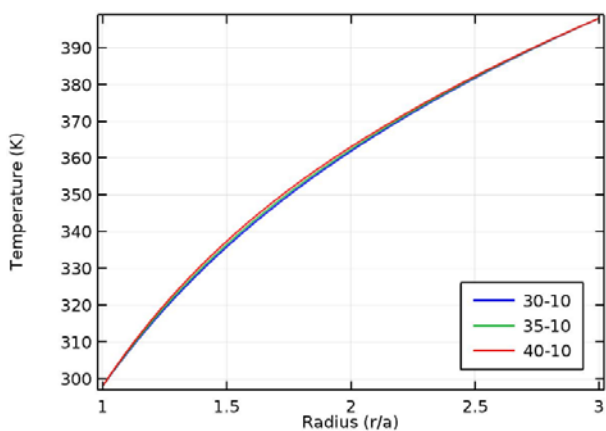


Figure 21. Increasing temperature profile over cylinder radius.

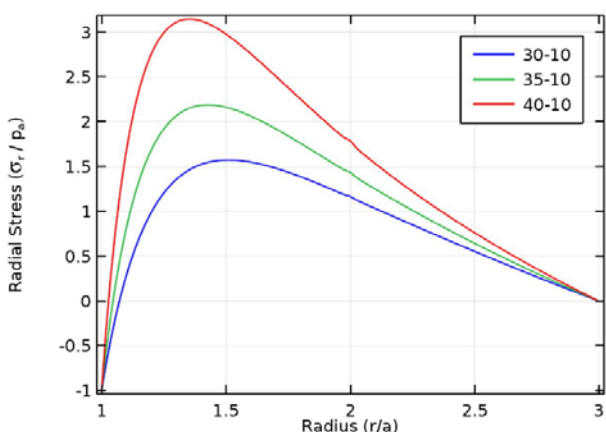


Figure 22. Radial stress under  $P_a = 25$  MPa,  $T_a = 298$  K,  $T_b = 398$  K.

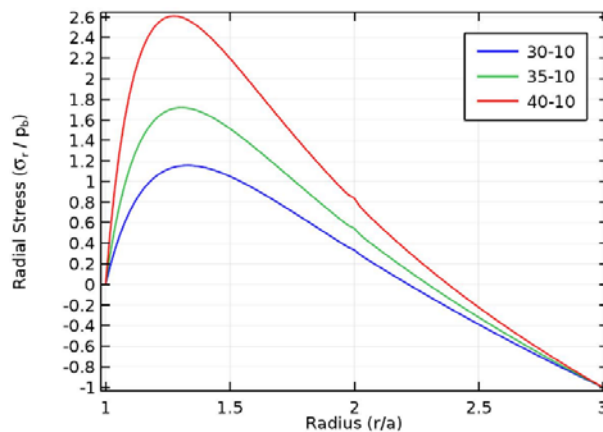


Figure 23. Radial stress under  $P_b = 25$  MPa,  $T_a = 298$  K,  $T_b = 398$  K.

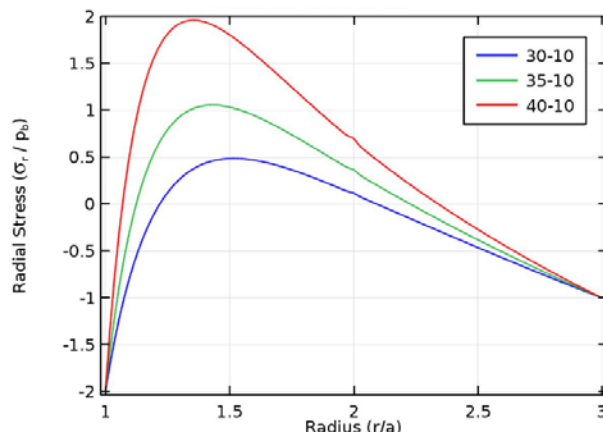


Figure 24. Radial stress:  $P_a = 50$  MPa,  $P_b = 25$  MPa,  $T_a = 298$  K,  $T_b = 398$  K.

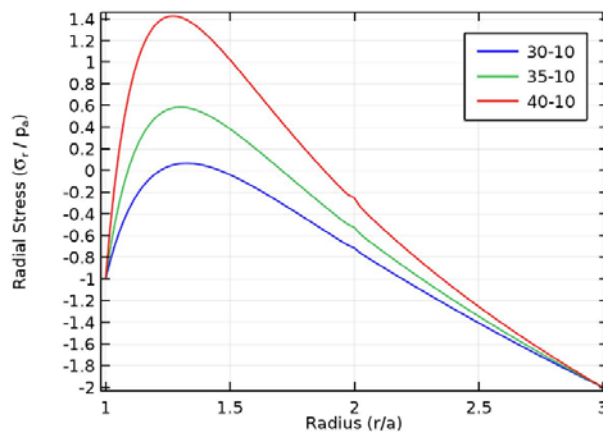


Figure 25 Radial stress:  $P_a = 25$  MPa,  $P_b = 50$  MPa,  $T_a = 298$  K,  $T_b = 398$  K.

Figures (26)-(29) depict tangential stress under combined effect of temperature loading, increasing from inner to outer radius, as well as pressure loading in the sandwich cylinder. Tangential stress with  $T_a = 298$  K,  $T_b = 398$  K and internal pressure  $P_a = 25$  MPa for different material composition as shown in Fig. (26), is tensile in nature and decreases along the radius of the cylinder and becomes compressive at external radius. Cylinder with 40-10 % reinforcement of  $\text{SiC}_p$  at inner and outer radii, in respect, has high tangential stress compared to cylinder with 30-10 % and 35-10 % reinforcement of  $\text{SiC}_p$  at inner and outer radii respectively. It is observed from Fig. (27), due to external pressure  $P_b =$

25 MPa, the tangential stress decreases at inner radius and becomes compressive along cylinder radius. Tangential stress under the combination of internal  $P_a = 50$  MPa and external pressure  $P_b = 25$  MPa, as depicted in Fig. (28), has decreased at inner radius, as compared to case of internal pressure only. It can be observed that due to compressive pressure applied at external radius, the tangential stress at external radial points tends to increase with negative magnitude. Figure (29) depicts the case when cylinder is under the effect of low internal  $P_a = 25$  MPa and high external pressure  $P_b = 50$  MPa. Clearly, tangential stress due to high external pressure gets shifted towards internal radii, with considerable decrease. Under the effect of temperature loading, the tangential stress in sandwich cylinder becomes tensile in nature with concave-up and decreasing trend in its magnitude along the cylinder radius, opposite to its behaviour under only mechanical loading effect.

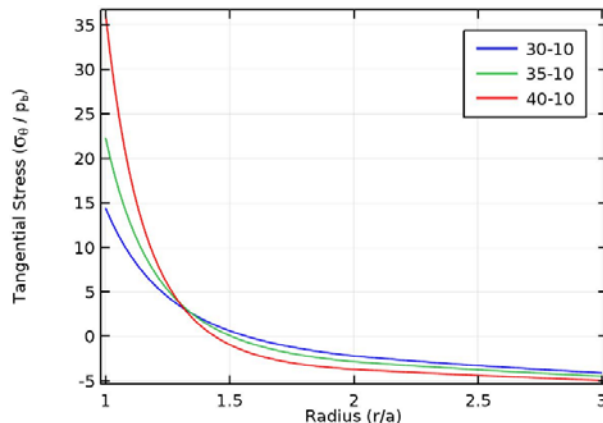


Figure 28. Tangential stress:  $P_a = 50$  MPa,  $T_a = 298$  K,  $T_b = 398$  K.

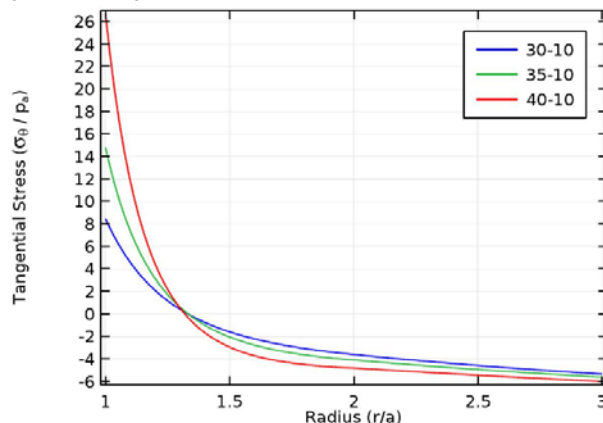


Figure 29. Tangential stress:  $P_a = 25$  MPa,  $P_b = 50$  MPa,  $T_a = 298$  K,  $T_b = 398$  K.

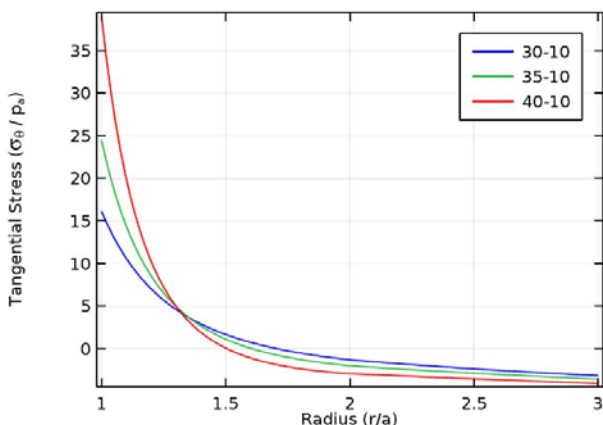


Figure 26. Tangential stress:  $P_a = 25$  MPa,  $T_a = 298$  K,  $T_b = 398$  K.

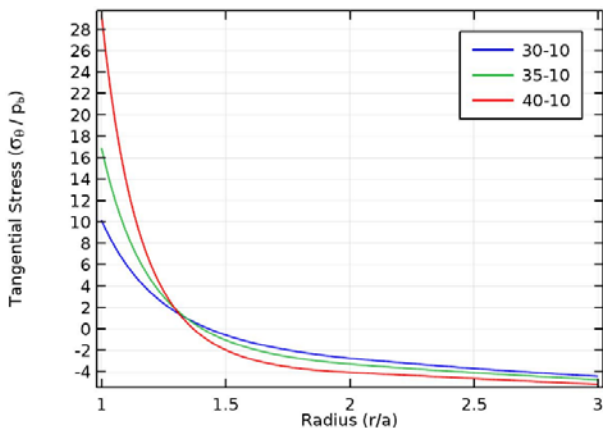


Figure 27. Tangential stress:  $P_b = 25$  MPa,  $T_a = 298$  K,  $T_b = 398$  K.

Figures (30)-(33) show the behaviour of displacement under increasing temperature profile. It can be observed from graphs of displacement, under effects of temperature and mechanical loading, the displacement increases from inner to outer radius of cylinder. The behaviour of displacement becomes concave up, as opposed to the concave down behaviour in the mechanical loading case.

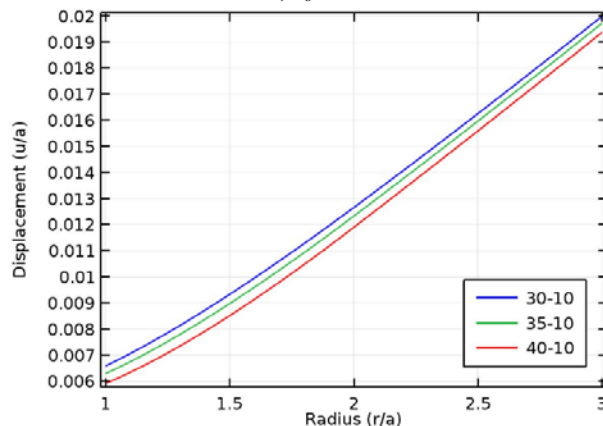


Figure 30. Displacement under  $P_a = 25$  MPa,  $T_a = 298$  K,  $T_b = 398$  K.

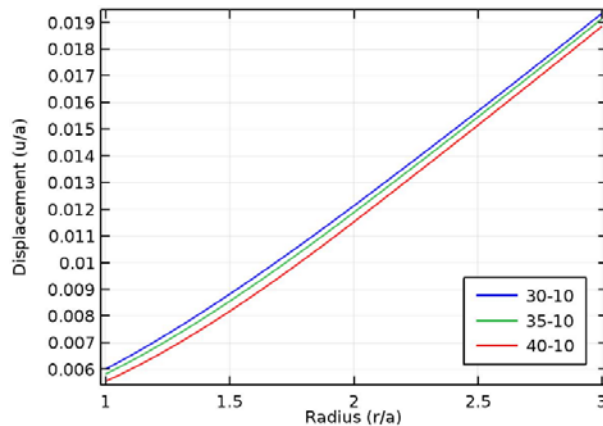


Figure 31. Displacement under  $P_b = 25$  MPa,  $T_a = 298$  K,  $T_b = 398$  K.

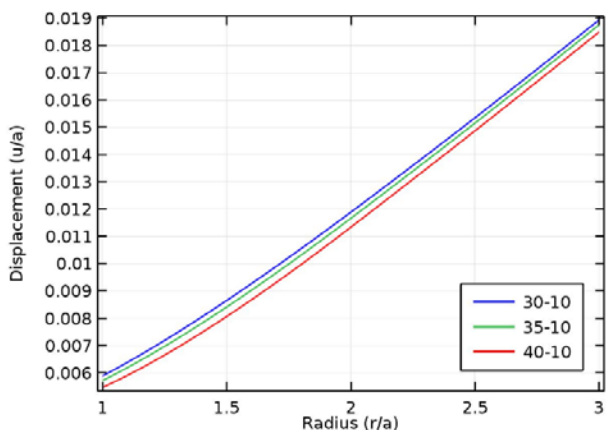


Figure 32 Displacement:  $P_a = 25 \text{ MPa}$ ,  $P_b = 50 \text{ MPa}$ ,  $T_a = 298 \text{ K}$ ,  $T_b = 398 \text{ K}$ .

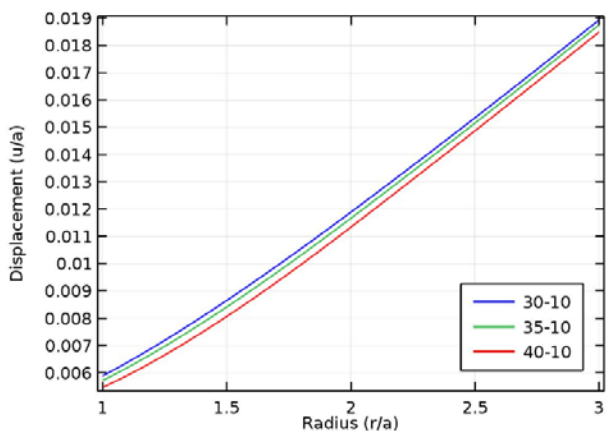


Fig. 33. Displacement:  $P_a = 50 \text{ MPa}$ ,  $P_b = 25 \text{ MPa}$ ,  $T_a = 298 \text{ K}$ ,  $T_b = 398 \text{ K}$ .

Figures (34)-(45) represent stresses and displacement under the effect of decreasing temperature profile from inner to external radius. From Fig. (35), it can be observed that radial stress is compressive in nature under decreasing thermal loading and internal pressure. The sandwich cylinder with 40-10 % reinforcement of  $\text{SiC}_p$  at inner and outer radii respectively has low radial stress at internal radii that further decreases considerably at outer radius with discontinuity at interface radius, due to material mismatch. But as observed in case of cylinder with 30-10 % and 35-10 % reinforcement of  $\text{SiC}_p$  at inner and outer radii, the radial stress is high which further increases at some internal radial points and starts to decrease towards the outer radius. It can also be noted that the radial stress is smoother as compared to 40-10 %  $\text{SiC}_p$  reinforcement. This behaviour is due to high modulus of elasticity which provides more resistance to the cylinder in order to withstand stress due to thermomechanical loading. As seen in Fig. (36), radial stress under thermo-mechanical loading with external pressure is again compressive in nature with an increase at the internal radius and a decrease at outer radial points. As compared to the case of internal pressure, radial stress is highly compressive under the effect of external pressure. Figure (37) shows radial stress under the combined effect of thermal loading with high internal ( $P_a = 50 \text{ MPa}$ ) together with low external ( $P_b = 25 \text{ MPa}$ ) pressure shows a similar trend as seen in Fig. (35) for internal pressure  $P_a = 25 \text{ MPa}$ . As observed from Fig. (36), radial stress under thermal loading with low

internal  $P_a = 25 \text{ MPa}$  and high external pressure  $P_b = 50 \text{ MPa}$  shifts towards internal radius. Also, a slight change in stress order of magnitude in the sandwich cylinder with different reinforcements can be seen. Figures (39)-(42) represent tangential stress under decreasing temperature profile and different pressure cases. Tangential stress in cylinder with 40-10 % reinforcement of  $\text{SiC}_p$  at inner and outer radii respectively, under internal pressure, as shown in Fig. (39), is tensile in nature which decreases along the internal radius but increases towards the outer radius with a singularity at interfacial radial point, whereas in case of cylinder with 30-10 % and 35-10 %  $\text{SiC}_p$  reinforcement at inner and outer radii, in respect, it is compressive in nature and decreases in magnitude along the cylinder radius.

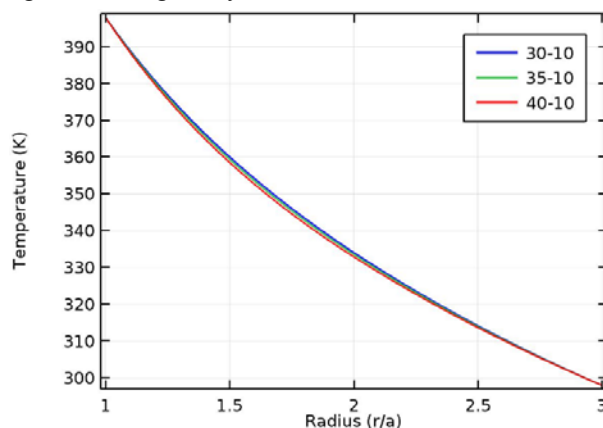


Figure 34. Decreasing temperature profile along cylinder radius.

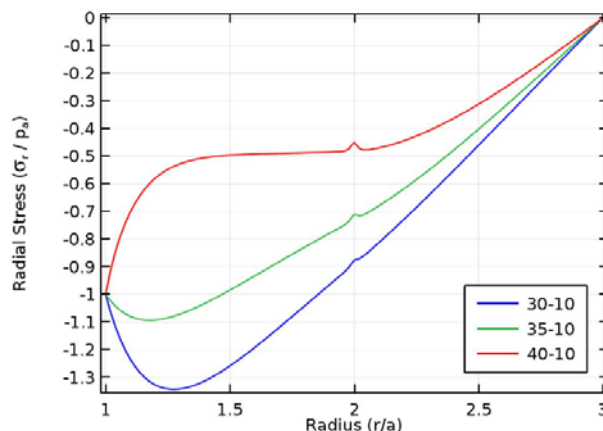


Figure 35. Radial stress:  $P_a = 25 \text{ MPa}$ ,  $T_a = 398 \text{ K}$ ,  $T_b = 298 \text{ K}$ .

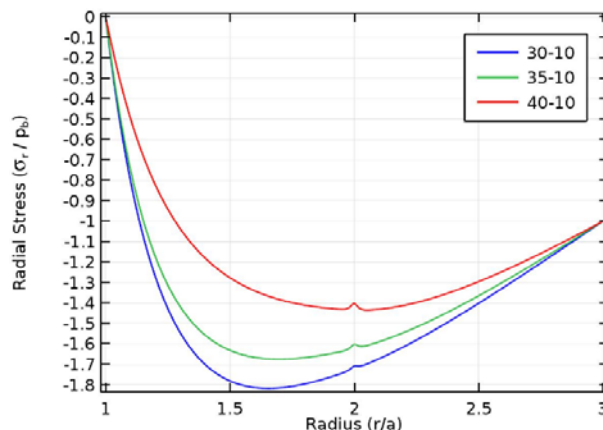


Figure 36. Radial stress:  $P_b = 25 \text{ MPa}$ ,  $T_a = 398 \text{ K}$ ,  $T_b = 298 \text{ K}$ .

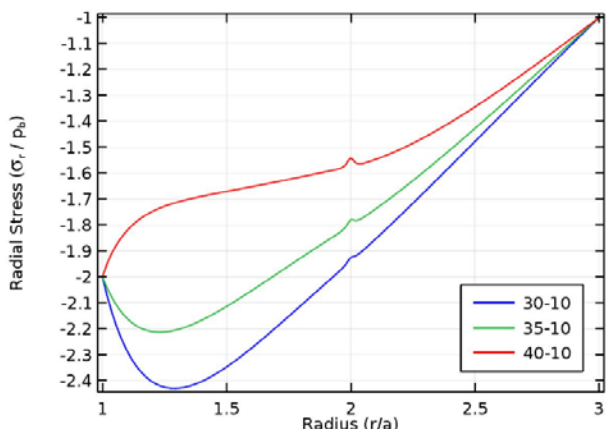


Fig. 37. Radial stress:  $P_a = 50 \text{ MPa}$ ,  $P_b = 25 \text{ MPa}$ ,  $T_a = 398 \text{ K}$ ,  $T_b = 298 \text{ K}$ .

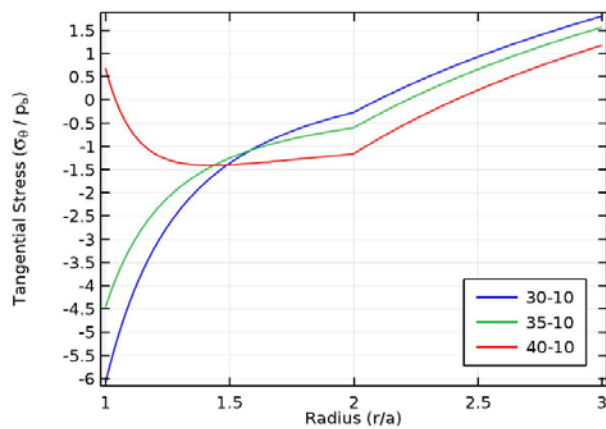


Fig. 41. Tangen. stress:  $P_a = 50 \text{ MPa}$ ,  $P_b = 25 \text{ MPa}$ ,  $T_a = 398 \text{ K}$ ,  $T_b = 298 \text{ K}$ .

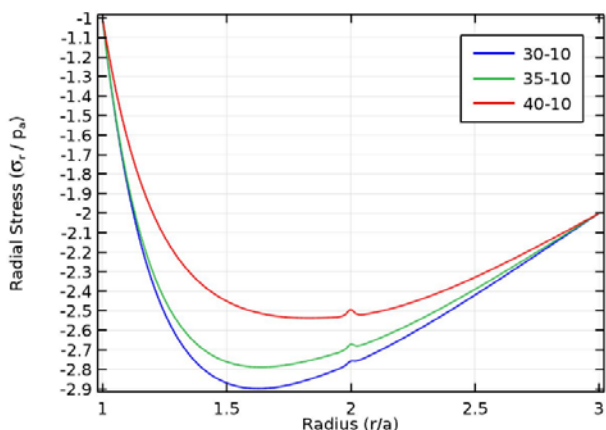


Fig. 38. Radial stress:  $P_a = 25 \text{ MPa}$ ,  $P_b = 50 \text{ MPa}$ ,  $T_a = 398 \text{ K}$ ,  $T_b = 298 \text{ K}$ .

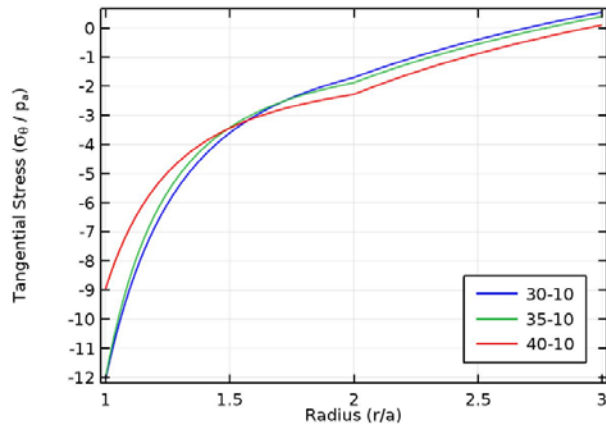


Fig. 42. Tangen. stress:  $P_a = 25 \text{ MPa}$ ,  $P_b = 50 \text{ MPa}$ ,  $T_a = 398 \text{ K}$ ,  $T_b = 298 \text{ K}$ .

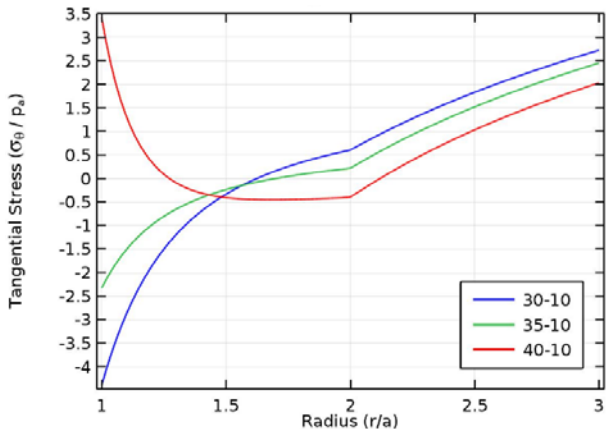


Figure 39. Tangential stress:  $P_a = 25 \text{ MPa}$ ,  $T_a = 398 \text{ K}$ ,  $T_b = 298 \text{ K}$ .

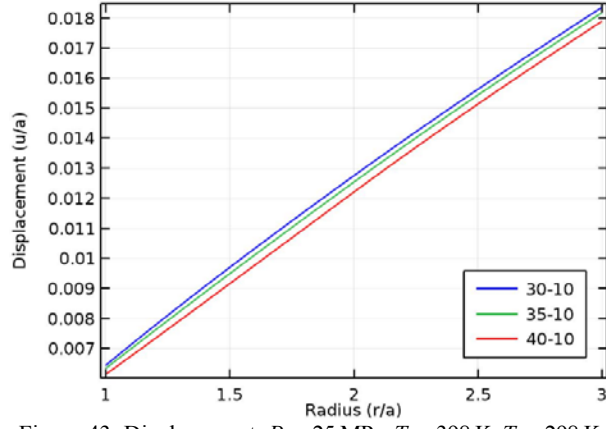


Figure 43. Displacement:  $P_a = 25 \text{ MPa}$ ,  $T_a = 398 \text{ K}$ ,  $T_b = 298 \text{ K}$ .

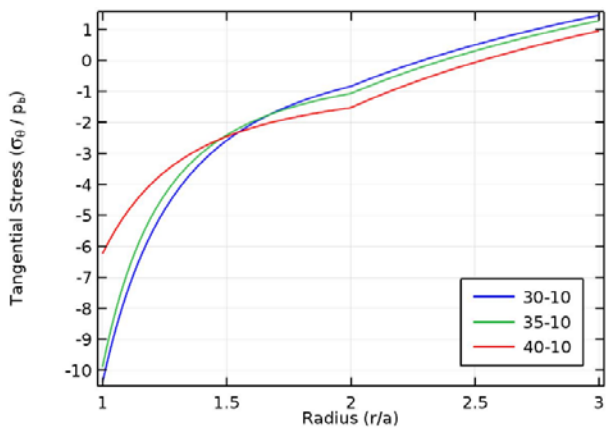


Figure 40. Tangential stress:  $P_b = 25 \text{ MPa}$ ,  $T_a = 398 \text{ K}$ ,  $T_b = 298 \text{ K}$ .

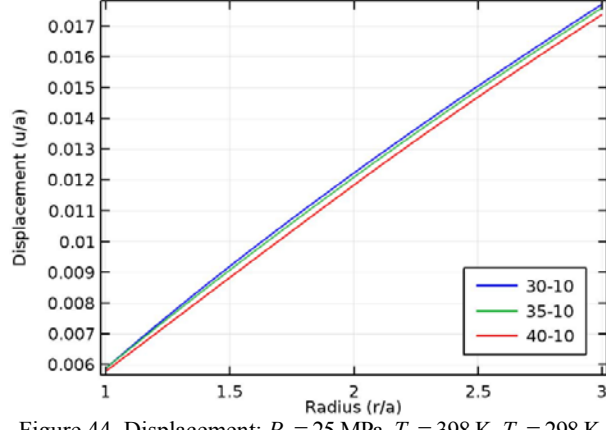


Figure 44. Displacement:  $P_a = 25 \text{ MPa}$ ,  $T_a = 398 \text{ K}$ ,  $T_b = 298 \text{ K}$ .

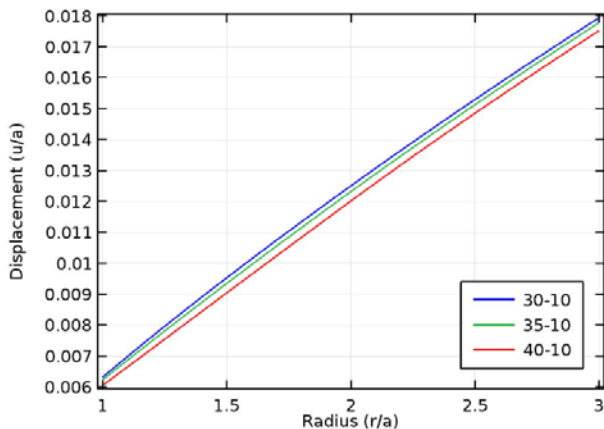


Fig. 45. Displacement:  $P_a = 50$  MPa,  $P_b = 25$  MPa,  $T_a = 398$  K,  $T_b = 298$  K.

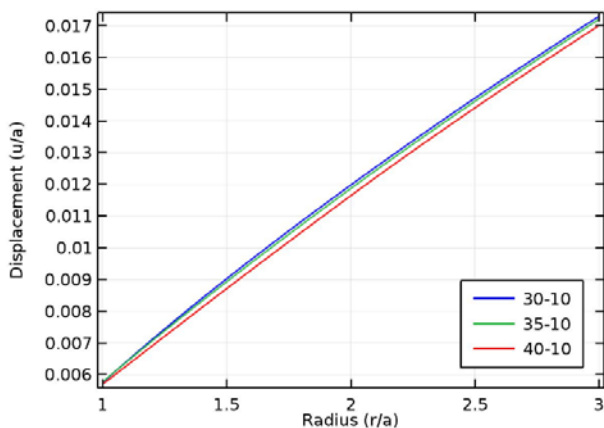


Fig. 46. Displacement:  $P_a = 25$  MPa,  $P_b = 50$  MPa,  $T_a = 398$  K,  $T_b = 298$  K.

Figure (40) indicates tangential stress in the sandwich cylinder under the effect of thermal loading and external pressure. Tangential stresses become compressive and uniform in case of all three material reinforcements. Also, the tangential stress decreases from internal to external radii. Figure (41) shows tangential stress under thermal loading as well as combined effect of high internal and low external pressure. The behaviour in this case is similar to the one observed in Fig. (39), with change in magnitude of tangential stress due to external pressure. From Fig. (42), it can be noted that tangential stress under low internal and high external pressure presents the same behaviour as shown in Fig. (39) with increase in its magnitude. Figures (43)-(46) depicts displacement in sandwich cylinder under thermal loading with different pressure cases. Displacement under decreasing thermal profile is tensile in nature with increasing trend from inner to outer radius. Displacement in all three cases of reinforcement is increasing uniformly from inner to outer radius. It can also be observed that sandwich cylinder with low magnitude of stress has least magnitude of displacement.

Thus, the conclusion of our analysis for sandwich cylinder under the effect of thermal and mechanical loading with inner layer made up of FGM and outer layer as composite is presented in the conclusion section.

## CONCLUSION

In our study, we considered the thick-walled sandwich cylinder with inner layer as functionally graded material and outer layer as composite material. Following findings can be concluded for thick-walled sandwich cylinder which is under the effect of mechanical as well as thermal loading:

- Material composition of sandwich cylinder has significant influence on the behaviour of radial and tangential stress under different pressure and thermal loading, as observed from results.
- Under effect of mechanical as well as thermomechanical loading, radial and tangential stresses show discontinuity at the interfacial layer that arise due to material mismatch at that point.
- Displacement in the sandwich cylinder under mechanical effect is of concave down form, but with the introduction of thermal loading, it increases uniformly from inner to the outer radius.

## REFERENCES

1. Seifi, R. (2015), *Exact and approximate solutions of thermo-elastic stresses in functionally graded cylinders*, J Thermal Stresses, 38(10): 1163-1182. doi: 10.1080/01495739.2015.1073513
2. Malekzadeh, P., Golbahar Haghghi, M.R., Heydarpour, Y. (2012), *Heat transfer analysis of functionally graded hollow cylinders subjected to an axisymmetric moving boundary heat flux*, Num. Heat Trans., Part A: Applic. 61(8): 614-632. doi: 10.1080/10407782.2012.670587
3. Hajisadeghian, A., Masoumi, A., Parvizi, A. (2018), *Investigating the magnetic field effects on thermomechanical stress behavior of thick-walled cylinder with inner FGM layer*, J Therm. Stresses, 41(3): 286-301. doi: 10.1080/01495739.2017.1399307
4. Thawait, A.K., Sondhi, L., Sanyal, S., Bhowmick, S. (2019), *Stress and deformation analysis of clamped functionally graded rotating disks with variable thickness*, Mech. Mechan. Eng. 23(1): 202-211. doi: 10.2478/mme-2019-0027
5. Nie, G.J., Batra, R.C. (2010), *Exact solutions and material tailoring for functionally graded hollow circular cylinders*, J Elasticity, 99(2): 179-201. doi: 10.1007/s10659-009-9239-8
6. Bayat, M., Rahimi, M., Saleem, M., et al. (2014), *One-dimensional analysis for magneto-thermo-mechanical response in a functionally graded annular variable-thickness rotating disk*, Appl. Math. Model. 38(19-20): 4625-4639. doi: 10.1016/j.apm.2014.03.008
7. Mehta, P.D., Sahni, M., Thakur, P. (2019), *Strength analysis of functionally graded rotating disc under variable density and temperature loading*, Struct. Integr. and Life, 19(2): 95-101.
8. Dini, A., Nematollahi, M.A., Hosseini, M. (2019), *Analytical solution for magneto-thermo-elastic responses of an annular functionally graded sandwich disk by considering internal heat generation and convective boundary condition*, J Sandwich Struct. & Mater.: doi: 10.1177/1099636219839161
9. Yildirim, S., Tutuncu, N. (2019), *Effect of magneto-thermal loads on the rotational instability of heterogeneous rotors*, AIAA Journal, 57(5): 2069-2074. doi: 10.2514/1.J058124
10. Sadrabadi, S.A., Rahimi, G.H., Citarella, R., et al. (2017), *Analytical solutions for yield onset achievement in FGM thick walled cylindrical tubes undergoing thermomechanical loads*, Compos. Part B: Eng., 116: 211-223. doi: 10.1016/j.compositesb.2017.02.023

11. Sharma, S., Yadav, S., Sharma, R. (2018), *Creep torsion in thick-walled circular cylinder under internal and external pressure*, Struct. Integr. and Life, 18(2): 89-97.
12. Sahni, M., Sahni, R., Mehta, P. (2017), *Creep behaviour under  $SiC_p$  exponential volume reinforcement in FGM composite rotating cylinders*, Mater. Today: Proc. 4(9): 9529-9533. doi: 10.1016/j.matpr.2017.06.218
13. Loghman, A., Parsa, H. (2014), *Exact solution for magneto-thermo-elastic behaviour of double-walled cylinder made of an inner FGM and an outer homogeneous layer*, Int. J Mech. Sci. 88: 93-99. doi: 10.1016/j.ijmecsci.2014.07.007
14. Loghman, A., Arani, A.G., Amir, S., Vajedi, A. (2010), *Magneto-thermoelastic creep analysis of functionally graded cylinders*, Int. J Press. Vess. Piping, 87(7): 389-395. doi: 10.1016/j.iipvp.2010.05.001
15. Celebi, K., Yarımpabuc, D., Keles, I. (2017), *A novel approach to thermal and mechanical stresses in a FGM cylinder with exponentially-varying properties*, J Theor. Appl. Mech. 55(1): 343-351. doi: 10.15632/jtam-pl.55.1.343
16. Kumar Paul, S., Sahni, M. (2019), *Two-dimensional mechanical stresses for a pressurized cylinder made of functionally graded material*, Struct. Integr. and Life, 19(2): 79-85.

© 2019 The Author. Structural Integrity and Life, Published by DIVK (The Society for Structural Integrity and Life 'Prof. Dr Stojan Sedmak') (<http://divk.inovacionicentar.rs/ivk/home.html>). This is an open access article distributed under the terms and conditions of the [Creative Commons Attribution-NonCommercial-NoDerivatives 4.0 International License](https://creativecommons.org/licenses/by-nc-nd/4.0/)

## ICSID 2020 – 4<sup>th</sup> International Conference on Structural Integrity and Durability

Fatigue and Fracture - Theory and Applications, September 15-18, 2020, and

Summer School, Fatigue and Fracture Modeling and Analysis, September 14-15, 2020

Dubrovnik, Croatia

The objective of the ICSID 2020 conference is to bring together scientists and engineers from around the world to discuss how to characterize, analyze, predict and assess the fatigue and fracture of structural materials and components. The ICSID 2020 intends to be a forum for discussion of the present and future trends in experimental, theoretical and applied fracture mechanics, fatigue, structural integrity assessment, failure analysis, and other important topics in the field.

### Conference topics

Advanced testing and evaluation techniques; Analytical Models; Applications to components and structures; Corrosion, environmentally enhanced degradation and cracking, corrosion fatigue; Cyclic deformation and crack initiation; Damage mechanics and models; Databases, expert systems and software; Durability and life extension of structures and components; Failure investigation and analysis; Failure of nanomaterials and nanostructures; Fatigue and fracture of polymers, elastomers, composites and biomaterials; Fatigue and fracture of weldments, welded components, joints and adhesives; Fatigue and fracture simulation and testing at all length scales; Fatigue crack path prediction; Finite elements methods and their application; Fracture and damage of cementitious materials; Fracture and failure criteria; Fretting fatigue and wear; Low, medium and high cycle fatigue; Macro scale fatigue prognosis techniques; Microstructure scale computational modeling; Mixed-mode and multiaxial fatigue and fracture; Models, criteria and methods in fracture mechanics; Multiscale materials modeling; Non-destructive evaluation (NDE); Probabilistic Fracture Mechanics; Reliability and integrity of engineering structures; Residual stress effects; Structural integrity assessment; Structural integrity of 3D-printed structures; Surface treatment and failure resistance improvement

### Conference venue

Centre for Advanced Academic Studies  
Don Frana Bulića 4, 20000 Dubrovnik, Croatia  
<http://www.caas.unizg.hr>

### Publications

Accepted abstracts will be published in the Book of Abstracts with an ISBN number. Full papers will be published on electronic media with permanent ISSN number 2584-3982. Authors of selected papers will be invited to submit extended versions for publication in a Special Issue of the *Engineering Failure Analysis*.

### Conference Chair

Željko Božić  
University of Zagreb  
Faculty of Mechanical Engineering and Naval Architecture  
Department of Aeronautical Engineering

### Deadlines

Abstract submission: May 1, 2020

Notification on abstract: within three weeks after receipt of abstract

Early registration: August 1, 2020

Submission of full paper (optional): August 1, 2020

### ICSID 2020 – SUMMER SCHOOL

The Summer School provides an opportunity for scientists, researchers and engineers from academia and industry to get acquainted with fundamental aspects of fracture mechanics, recent trends in practical applications of fatigue and fracture models, and advanced approaches such as multiscale materials modelling. Leading scientists and experts will give lectures on experimental and numerical techniques for modelling, analysis and assessment of damaged components and structures.

### Contact

Prof. dr. sc. Željko Božić, ICSID 2020 Chair  
Phone: +385 1 6168536, Mobile: +385 98 1863915  
Fax: +385 1 6156940, [zeljko.bozic@fsb.hr](mailto:zeljko.bozic@fsb.hr)  
Faculty of Mechanical Engineering and Naval Architecture  
Ivana Lučića 5, 10000 Zagreb, Croatia  
Email: [icsid@fsb.hr](mailto:icsid@fsb.hr)

### More info

<http://icsid2020.fsb.hr>

